Disorder-induced topological state transition in the optical skyrmion family

Changxu Liu*
Department of Mathematics, Physics and Electrical Engineering, Northumbria University, Newcastle Upon Tyne NE1 8ST, United Kingdom
Chair in Hybrid Nanosystems, Nanoinstitute Munich, Faculty of Physics, Ludwig-Maximilians-Universitaet Muenchen, 80539 Muenchen, Germany

Shuang Zhang
Department of Physics, University of Hong Kong, Hong Kong, China
Department of Electrical Engineering, University of Hong Kong, Hong Kong, China

Stefan A. Maier
School of Physics and Astronomy, Monash University, Clayton, Victoria 3800, Australia
Chair in Hybrid Nanosystems, Nanoinstitute Munich, Faculty of Physics, Ludwig-Maximilians-Universitaet Muenchen, 80539 Muenchen, Germany
Department of Physics, Imperial College London, London SW7 2AZ, UK

Haoran Ren†
School of Physics and Astronomy, Monash University, Clayton, Victoria 3800, Australia
(Dated: December 8, 2022)

Skyrmions endowed with topological protection have been extensively investigated in various platforms including magnetics, ferroelectrics and liquid crystals, stimulating applications such as memories, logic devices and neuromorphic computing. While the optical counterpart has been proposed and realised recently, the study of optical skyrmions is still in its infancy. Among the unexplored questions, the investigation of the topology-induced robustness against disorder is of substantial importance on both fundamental and practical sides but remains elusive. In this letter, we manage to generate optical skyrmions numerically in real space with different topological features at will, providing a unique platform to investigate the robustness of various optical skyrmions. A disorder-induced topological state transition is observed for the first time in a family of optical skyrmions composed of six classes with different skyrmion numbers. Intriguingly, the optical skyrmions produced from a vectorial hologram are exceptionally robust against scattering from a random medium, shedding light on topological photonic devices for the generation and manipulation of robust states for applications including imaging and communication.

I. INTRODUCTION

Skyrmions, originally proposed by Skyrme in the 1960s to describe the stability of the constituents of elementary particles[1], are vortex-like formations of a field that cannot be eliminated by any smooth transformation. After first realisations in magnetic systems [2–6], the topology-otected quasiparticles have been achieved in fundamentally different classical and quantum platforms, ranging from liquid crystals[7–10], ferroelectrics[11–14] to polariton superfluids [15] and acoustics [16].

Recently, the photonic counterpart of skyrmions has been first realised in surface plasmon polaritons [17], utilising the evanescent electric field to form the desired topology. Later, optical skyrmions were achieved in a repertoire of systems based on different vector fields, including electric[18] or magnetic[19, 20] fields in real space and photonic spin/Stokes vectors in artificial space[21–28]. In analogy with Dzyaloshinskii Moriya interaction in magnetic skyrmion [2–6], various types of light mater interactions, including spin-orbit coupling [21–23], photonic quantum spin Hall effect [25] and artificial photonic gauge field [24], were utilised to form vectorial fields matching the topology of a specific class of skyrmions. Meanwhile, optical skyrmions free from interaction with materials can be achieved in free space through the superposition of structured light [20, 26–29]. Néel and Bloch-type optical skyrmions have been proposed in the polarisation fields [29]. Optical skyrmions with different topologies have been realised from a digital hologram system based on Stokes vector fields in the artificial space [27], providing flexibility not achieved by the magnetic counterpart.

In magnetic systems, the non-trivial topology endows skyrmion with unparalleled robustness to perturbation, suggesting a platform for various applications such as memory, logic devices and neuromorphic computing [4, 30, 31]. While the robustness of magnetic skyrmions has been extensively studied [32–45], a systematic investigation of optical skyrmions with the presence of disorder remains elusive. A comprehensive understanding of robustness is indispensable for the further progress of optical skyrmions, aiming at practical applications including

* changxu.liu@northumbria.ac.uk
† haoran.ren@monash.edu

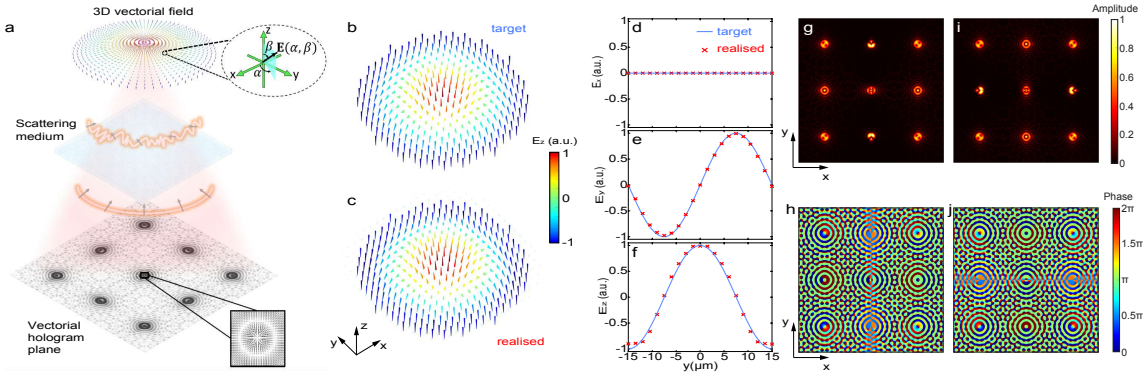

FIG. 1. (color online). Realisation of the Néel-type skyrmion. (a) Artistic view of a vectorial hologram for creating an optical skyrmion that is digitised by 3D vectorial fields in real space. Fluctuations in amplitude and phase can be introduced from the scattering medium. (b) An ideal Néel-type skyrmion ($N_{\rm sk} = 1, \nu = 1, h = 0$). (c) The realised quasiparticle composed of vectorial electric field. (d-f) A comparison of the electric field in the symmetric axis. (g-j) The designed amplitude and phase on the hologram plane, i.e., the bottom plane shown in (a). The amplitude and phase polarised along the x-direction are shown in g) and h), while the amplitude and phase polarised along the y-direction are shown in i) and j).

imaging, microscopy, communication and encryption[46].

Inspired by recent advances in the manipulation of three-dimensional (3D) vectorial fields [47–52], we propose a novel platform for the realisation of arbitrary optical skyrmions in real space. Quasiparticles with different skyrmion numbers[53] ($N_{\rm sk} = 1, -1, \frac{1}{2}, \frac{1}{4}$) are achieved numerically based on the electric field vectors from a vectorial hologram. More importantly, we provide a comprehensive investigation of the robustness against disorder, accounting for the imperfection of hologram devices or light propagation in a scattering medium. To the best of our knowledge, we report here the first disorder-induced state transition in optical skyrmions. The state transition is confirmed as a general phenomenon for a family of quasiparticles, ranging from anti-skyrmions, skyrmions to half- and quarter- skyrmions. Surprisingly, the unique topology of skyrmion endows the optical quasi-particle with an unprecedented robustness against disorder in phase, maintaining the nontrivial feature under fluctuations up to 0.7π. Our work not only contributes to the fundamental physics by offering the first comparison of the disorder-induced state transition for the skyrmion family, but also sheds light on practical applications such as imaging and communications for optical skyrmions where the random scattering is inevitable.

II. RESULTS

The physical mechanism of using a vectorial hologram for creating arbitrary optical skyrmions is illustrated in Fig. 1a. Based on the principle of 3D vectorial holography [48], these 3D vectorial fields at given positions in the image plane can be physically determined from a 2D vector field distribution in the hologram plane. A 3D vectorial field is represented by $E(\alpha, \beta)$ in a spherical coordinate system, where α and β are the azimuthal and polar angles, respectively (inset of Fig. 1a). We use the generalised vectorial diffraction theory to evaluate the orthogonal electric field components (E_x, E_y, E_z) of a 3D vectorial field under the tight focusing condition, which can independently correlate the orthogonal electric field components of the 3D vectorial field $E(\alpha, \beta)$ with different azimuthal and radial components of a 2D vector field in the hologram plane. More details can be found in Supplementary Material [54].

Utilising the vectorial hologram, we are able to achieve a 3D electric field texture point by point on the 2D image plane, and produce the desired configuration matching the topology of optical skyrmions. The topological property of a 2D quasiparticle is characterised by the skyrmion number defined as

$$N_{\rm sk} = \frac{1}{4\pi} \iint_S \mathbf{n} \cdot \left(\frac{\partial \mathbf{n}}{\partial x} \times \frac{\partial \mathbf{n}}{\partial y} \right) \mathrm{d}x \ \mathrm{d}y \qquad (1)$$

with the vector field $\mathbf{n}$ forming a quasiparticle constrained in a 2D region S. A nontrivial skyrmion number counts the number of winding for vectors going from centre to boundary. Accompanying the skyrmion number, the vorticity number (ν) and the helicity number (h) are introduced for a complete characterisation of a skyrmion[53]. Three distinct values of $(N_{\rm sk}, \nu, h)$ differentiate a particular class of quasiparticle from the skyrmion family. More details can be found in Supplementary Material [54].

Figures 1b-j summarise the realisation of a Néel-type skyrmion based on the proposed vectorial hologram. An ideal Néel-type skyrmion is illustrated in Fig. 1b. The arrow represents the electric field, and its colour measures the magnitude of E_z. The quasiparticle has an axisymmetric texture, with the electric field vector rotating radially from downwards to upwards pointing. Figure 1c shows the 3D electric field realised. Discrete points from the skyrmion are selected and produced through

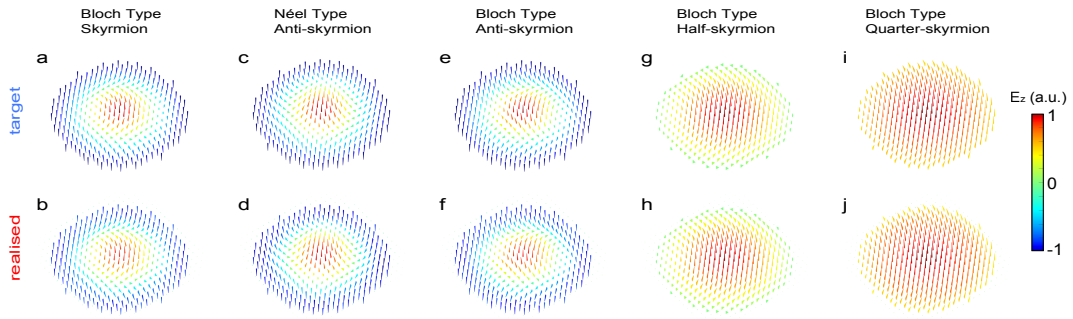

FIG. 2. (color online) Realisation of different classes of optical skyrmions based on vectorial hologram. The first row demonstrates the ideal textures and the second row shows the realised quasiparticles composed of vectorial electric field. Five classes are included: (a-b) Bloch-type skyrmion ($N_{\rm sk} = 1, \nu = 1, h = \frac{\pi}{2}$); (c-d) Néel-type anti-skyrmion ($N_{\rm sk} = 1, \nu = -1, h = 0$); (e-f) Bloch-type anti-skyrmion ($N_{\rm sk} = 1, \nu = -1, h = \frac{\pi}{2}$); (g-h) Bloch-type half-skyrmion ($N_{\rm sk} = \frac{1}{2}, \nu = 1, h = \frac{\pi}{2}$); (i-j) Bloch-type quarter-skyrmion ($N_{\rm sk} = \frac{1}{4}, \nu = 1, h = \frac{\pi}{2}$).

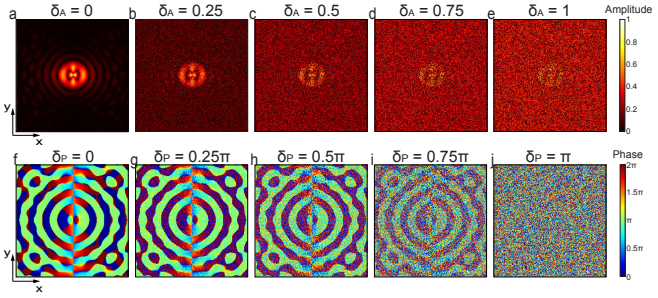

FIG. 3. (color online). A demonstration of disorder introduced in amplitude (a-e) and phase (f-j) on the hologram plane. The amplitude and phase are selected from the central region in Fig. 1f and g.

the vectorial hologram. The accuracy is confirmed by a comparison between the textures in Figure 1b and c with a negligible difference. We further provide a quantitative comparison in Fig. 1d to f, where the electric fields in three orthogonal directions are shown respectively. The field distribution along the symmetric axis y is selected, with solid blue lines for an ideal skyrmion and red crosses for the realised one. The zero helicity induces no field along x, while both E_y and E_z follow a sinusoidal-shaped curve. Despite differences between the target and realisation, the topological feature is well reproduced. The skyrmion number $N_{\rm sk}$ is numerically calculated based on Eq. 1, with region S defined as the circle with radius of 15 μm. The value of the realised Néel-type skyrmion is 0.98, close to the ideal value of 1. To realise the field texture shown in Fig. 1c, we utilise a vectorial hologram along both x and y polarisations. The designed amplitude and phase are demonstrated in Fig. 1g-j.

To demonstrate the versatility of the proposed method, we realised another five classes of skyrmions with distinct textures. Figure 2a shows a skyrmion of Bloch-type with a nonzero helicity $h = \frac{\pi}{2}$. Compared with Néel-type with the same values of $N_{\rm sk}$ and ν (Fig. 1a), it has a chiral feature in the x-y plane. Meanwhile, anti-skyrmions, quasiparticles with the opposite sign of $N_{\rm sk}$, are shown in Fig. 2c and e. Compared to their counterparts (Fig. 1b and Fig. 2a), the sign of the vorticity number is reversed from 1 to -1, while the value of h decides whether it is a Néel- or Bloch-type. In addition to quasiparticles with integer topological numbers, we further choose two classes of textures with fractional skyrmion numbers; the half-skyrmion (or merons) with $N_{\rm sk} = \frac{1}{2}$ and the quarter-skyrmion with $N_{\rm sk} = \frac{1}{4}$. The vector field only rotates a portion of a complete swap from downwards to upwards when approaching the centre (Fig. 2g and i). More details can be found in Supplementary Material [54]. All realised electric field textures (second row of Fig. 2) replicate the desired topology (first row of Fig. 2). The perfect match is confirmed quantitatively by the calculated (ideal) skyrmion numbers; 0.99(1) for Bloch-type skyrmion, -0.98(-1) for Néel-type anti-skyrmion, -0.99(-1) for Bloch-type anti-skyrmion, 0.504(0.5) for Bloch-type half-skyrmion and 0.247(0.25) for Bloch-type quarter-skyrmion. The calculated phase and amplitude in the hologram plane for all five classes can be found in Supplementary Material [54].

With the flexibility to produce a family of skyrmions, we implement a comprehensive investigation to elucidate how disorder can impair topological-protected quasiparticles. We introduce two types of disorder in our vectorial hologram: the fluctuations in phase and amplitude. Correspondingly, the amplitude $A(x, y)$ and phase $P(x, y)$ on the hologram plane (x, y) can be modelled as:

$$\begin{aligned} A(x, y) &= A_0(x, y) + \delta_A U_1(x, y) \\ P(x, y) &= P_0(x, y) + \delta_P U_2(x, y) \end{aligned} \tag{2}$$

with $A_0(x, y)$ and $P_0(x, y)$ the computed amplitude and phase, $U_{1,2}(x, y)$ independent uniform distributions within [-1, 1]. The value of δ_A (δ_P) represents a random fluctuation in the amplitude (phase), serving as a measurement of the strength of the disorder. Figure 3 shows the amplitude and phase distributions with vari-

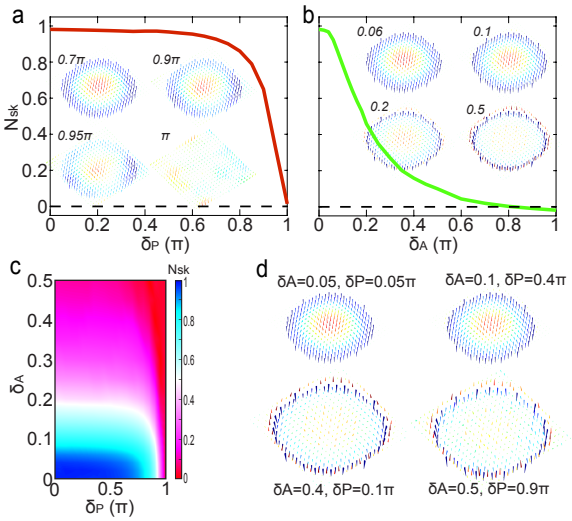

FIG. 4. (color online). Disorder-induced state transition of a Néel-type skyrmion. (a) The evolution of the skyrmion number $N_{\rm sk}$ as the increment of disorder in phase δ_P. δ_A is set to 0. The insets show the vectorial electric field textures under different values of δ_P. (b) The evolution of the skyrmion number $N_{\rm sk}$ as the increment of disorder in amplitude δ_A. δ_P is set to 0. The insets show the vectorial electric field textures under different values of δ_A. (c) The evolution of the skyrmion number $N_{\rm sk}$ when disorder in phase and amplitude coexists. (d) Demonstration of the textures of vectorial electric field with hybrid disorder.

ous levels of disorder. Figures 3a-e illustrate the distributions of amplitude with different values of δ_A, while Figs. 3f-j show the distributions of phase. The original amplitude (Figs. 3a) and phase (Figs. 3f) are chosen from the central part of Fig. 1f and g respectively. For both amplitude and phase, the increment of the fluctuation obscures the well-defined pattern and consequently impairs the skyrmions on the image plane.

Figure 4 summarises the robustness of a Néel-type skyrmion against fluctuations, demonstrating the disorder-induced state transition. To make a quantitative analysis, we calculate the skyrmion number $N_{\rm sk}$ of the electric vectorial field texture formed on the image plane. Figure 4a shows the situation with the fluctuation only in phase. When δ_A increases from 0 to π, the skyrmion number experiences a prominent degradation from 1 to 0. The value of 1 represents an ideal skyrmion, while zero refers to a fully randomised pattern. Interestingly, we observe strong robustness against phase disorder. The $N_{\rm sk}$ maintains its original value when $\delta_P < 0.7\pi$, decreasing from 0.98 to 0.92. Further increment of disorder in phase induces a sharp degradation. The four insets in Fig. 4a are the electric field distributions under different values of δ_P, demonstrating the state transition from a Néel-type skyrmion to a fully-randomised pattern.

The evolution of the skyrmion with the disorder in amplitude is shown in Figure 4b with δ_P=0. Again, we observe a disorder-induced state. However, the skyrmion is vulnerable to the disorder in amplitude. Similarly, we demonstrate the electric field distributions as the insets in Fig. 4b. The amplitude fluctuation has an intense impact on the edge of the skyrmion. Large δ_A randomises the electric field on the edge and results in the degradation of $N_{\rm sk}$.

We further investigate the case when both the fluctuation in phase and amplitude exist, with the results summarised in Fig. 4c-d. Figure 4c shows the evolution of N_{sk} as the increment of the two different types of disorder. The colour in the (δ_P, δ_A) plane represents the value of $N_{\rm sk}$, unequivocally showing a state transition from blue ($N_{sk} = 1$) to red (N_{sk}=0) as disorder increases. Topological protection is confirmed by the region with bluish colour, representing a minor degradation of the topological number ($N_{\rm sk} > 0.9$). We depict the four textures of the skyrmions when the hybrid disorder exists. The key features are kept when the value of δ_A is small, despite the moderate level of fluctuation in phase. The increase of δ_A can rapidly diminish the topological texture.

We attribute the robustness of the skyrmion to the unique topology in the hologram plane as shown in Fig. 1g-j. Holes or rings with near-zero values occurs inside the bright spots from the amplitude distribution, driving the shape topological nontrivial. Compared with amplitude-only disorder, the phase-only disorder applied on the whole x-y plane does not break the ring and hole topology existing in the amplitude plane, leading to strong robustness as shown in Fig. 4a-b. More details can be found in Supplementary Material [54].

We carry out similar systematic analyses for the robustness of the other five classes of skyrmions. The transition dynamics share a strong similarity with the Néel-type case, as shown in Supplementary Material [54]. A comparison of topological protection among these quasi-particles can be found in Supplementary Material [54].

In the previous analysis, we treat the disorder in amplitude and phase as independent random variables with uniform distribution, to study the impact separately. For the sake of practical applications where the amplitude and phase are intertwined, we further investigate the randomised phase and amplitude from scattering medium. To provide a comprehensive picture, two types of random media are included, with permittivity (ε) either varying discretely (Fig. 5a) or continuously (Fig. 5b). Correspondingly, the disorder in the medium can be controlled by the permittivity of the scatters ($\varepsilon_{\rm sca}$) in discrete random medium, or the standard deviation of the permittivity in continuous random medium (Δ_ε). By solving the Maxwell's equations numerically, we obtain the fluctuations of amplitude and phase from the realistic random medium. Similarly, the disorder of amplitude and phase can be applied to the hologram plane to test the robustness of the optical skyrmions by the evolution of the topological number $N_{\rm sk}$. The results are summarised in Fig. 5b and e, for all six types of skyrmions. Here, we use the absolute value of $N_{\rm sk}$, so the anti-skyrmions also

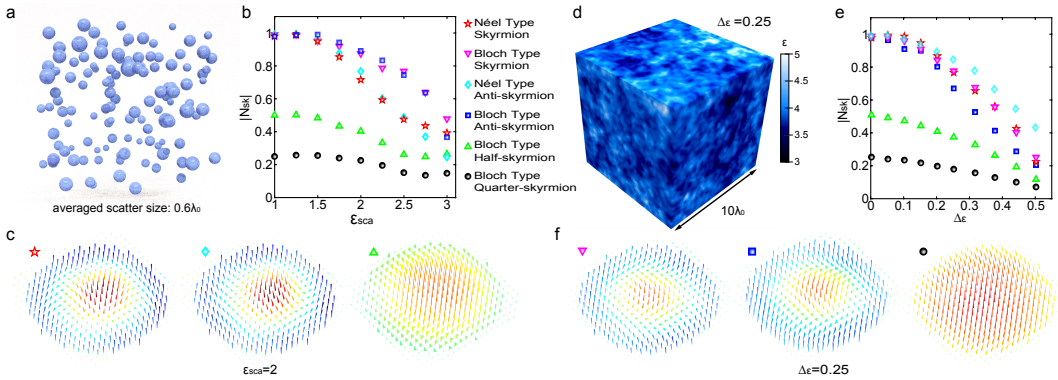

FIG. 5. (color online). The robustness of the optical skyrmions propagating through a random medium. (a)Demonstration of a discrete random medium. (b)The relationship between the absolute value of $N_{\rm sk}$ and the permittivity of the scatters $\varepsilon_{\rm sca}$ (c)The vectorial electric field textures when $\varepsilon_{\rm sca} = 2$. (d)Demonstration of a continuous random medium. (e)The relationship between the absolute value of $N_{\rm sk}$ and the standard deviation of dielectric function Δ_ε (f) The vectorial electric field textures when $\Delta_\varepsilon = 0.25$.

have positive topological numbers. We observe a strong robustness of skyrmions against the random scattering either from homogeneous medium dispersed with scatters or medium with permittivity fluctuations. In Fig. 5c and f, we depict the vectorial field of six skyrmions when going through medium with strong scattering ($\varepsilon_{\rm sca} = 2$ and $\Delta_\varepsilon = 0.25$). In spite of some distortion, the topological feature is unambiguously preserved. More details can be found in Supplementary Material [54].

III. DISCUSSION

Taking full advantages of the design flexibility of vectorial holograms, we manage to numerically realise arbitrary skyrmions in real space through the topological texture of the 3D vectorial fields on a two-dimensional plane. Not limited by the six classes of skyrmions demonstrated, other quasiparticles in the skyrmions family can be achieved through our concept, such as biskyrmion, skyrmioniums, bimeron or even quasiparticles in three-dimension[53]. The ability to produce quasiparticles in the same platform endows the possibility for a systemic comparison of the topological protection among different types of skyrmions, an important topic not covered previously neither in optics nor in magnetics. A universal disorder-induced topological state transition is demonstrated for all six classes. More importantly, we observe an unprecedented robustness endowed by the skrymions' topology against scattering from random medium either with scatters or continuously varying permittivity.

This discovery may shed light on both fundamental physics and practical applications, inspiring additional research in skyrmions and beyond. The robustness comparison among skyrmions with different topologies will be an interesting question in other systems in optics, magnetics and beyond, guiding the related applications with a demand for better immunity against imperfection. Also, the robustness embedded in optical skyrmions against phase and amplitude fluctuations from a scattering medium may stimulate a new generation of photonic devices producing structured light with unique topology. The immunity against disorder in phase and amplitude ensures the skyrmion keep its topological feature after going through a random media with moderate disorder, offering new possibilities for optical communications and image.

Meanwhile, the disorder can be modelled as the imperfection on the hologram device. In this scenario, a topological hologram texture is achieved with super robustness against phase fluctuations, with a sharp contrast with the existing holograms. This may stimulate future development of topological holograms based on ultrathin metasurfaces, the latter have recently transformed the photonic design [56–62].

S. A. M. acknowledges financial support from Deutsche Forschungsgemeinschaft Cluster of Excellence e-conversion (EXC 2089111-390776260), and the Lee-Lucas Chair in Physics. H. R. acknowledges funding support from the DECRA Project (DE220101085) from the Australian Research Council. S.Z the acknowledges financial support from Research Grants Council of Hong Kong (AoE/P-502/20).

[1] T. H. R. Skyrme, Nuclear Physics **31**, 556 (1962).
[2] N. Nagaosa and Y. Tokura, Nature Nanotechnology **8**, 899 (2013).
[3] R. Wiesendanger, Nature Reviews Materials **1**, 16044 (2016).
[4] A. Fert, N. Reyren, and V. Cros, Nature Reviews Mate-

rials , 17031 (2017).
[5] A. N. Bogdanov and C. Panagopoulos, Nature Reviews Physics **2**, 492 (2020).
[6] Y. Tokura and N. Kanazawa, Chemical Reviews **121**, 2857 (2020).
[7] I. I. Smalyukh, Y. Lansac, N. A. Clark, and R. P. Trivedi, Nature Materials **9**, 139 (2010).
[8] D. Foster, C. Kind, P. J. Ackerman, J.-S. B. Tai, M. R. Dennis, and I. I. Smalyukh, Nature Physics **15**, 655 (2019).
[9] A. Duzgun and C. Nisoli, Phys. Rev. Lett. **126**, 047801 (2021).
[10] J. Pišljar, S. Ghosh, S. Turlapati, N. V. S. Rao, M. Škarabot, A. Mertelj, A. Petelin, A. Nych, M. Marinčič, A. Pusovnik, M. Ravnik, and I. Muševič, Phys. Rev. X **12**, 011003 (2022).
[11] I. I. Naumov, L. Bellaiche, and H. Fu, Nature **432**, 737 (2004).
[12] Y. Nahas, S. Prokhorenko, L. Louis, Z. Gui, I. Kornev, and L. Bellaiche, Nature Communications **6**, 8542 (2015).
[13] S. Das, Y. L. Tang, Z. Hong, M. A. P. Gonçalves, M. R. McCarter, C. Klewe, K. X. Nguyen, F. Gómez-Ortiz, P. Shafer, E. Arenholz, V. A. Stoica, S. L. Hsu, B. Wang, C. Ophus, J. F. Liu, C. T. Nelson, S. Saremi, B. Prasad, A. B. Mei, D. G. Schlom, J. Íñiguez, P. García-Fernández, D. A. Muller, L. Q. Chen, J. Junquera, L. W. Martin, and R. Ramesh, Nature **568**, 368 (2019).
[14] S. Das, Z. Hong, V. Stoica, M. Gonçalves, Y.-T. Shao, E. Parsonnet, E. J. Marksz, S. Saremi, M. McCarter, A. Reynoso, *et al.*, Nature Materials **20**, 194 (2021).
[15] S. Donati, L. Dominici, G. Dagvadorj, D. Ballarini, M. De Giorgi, A. Bramati, G. Gigli, Y. G. Rubo, M. H. Szymańska, and D. Sanvitto, Proceedings of the National Academy of Sciences **113**, 14926 (2016).
[16] H. Ge, X.-Y. Xu, L. Liu, R. Xu, Z.-K. Lin, S.-Y. Yu, M. Bao, J.-H. Jiang, M.-H. Lu, and Y.-F. Chen, Physical Review Letters **127**, 144502 (2021).
[17] S. Tsesses, E. Ostrovsky, K. Cohen, B. Gjonaj, N. Lindner, and G. Bartal, Science **361**, 993 (2018).
[18] T. J. Davis, D. Janoschka, P. Dreher, B. Frank, F.-J. Meyer zu Heringdorf, and H. Giessen, Science **368**, eaba6415 (2020).
[19] Z.-L. Deng, T. Shi, A. Krasnok, X. Li, and A. Alù, Nature Communications **13**, 1 (2022).
[20] Y. Shen, Y. Hou, N. Papasimakis, and N. I. Zheludev, Nature Communications **12**, 1 (2021).
[21] L. Du, A. Yang, A. V. Zayats, and X. Yuan, Nature Physics **15**, 650 (2019).
[22] Y. Dai, Z. Zhou, A. Ghosh, R. S. Mong, A. Kubo, C.-B. Huang, and H. Petek, Nature **588**, 616 (2020).
[23] X. Lei, A. Yang, P. Shi, Z. Xie, L. Du, A. V. Zayats, and X. Yuan, Physical Review Letters **127**, 237403 (2021).
[24] M. Król, H. Sigurdsson, K. Rechcińska, P. Oliwa, K. Tyszka, W. Bardyszewski, A. Opala, M. Matuszewski, P. Morawiak, R. Mazur, *et al.*, Optica **8**, 255 (2021).
[25] Q. Zhang, Z. Xie, L. Du, P. Shi, and X. Yuan, Physical Review Research **3**, 023109 (2021).
[26] Y. Shen, Optics Letters **46**, 3737 (2021).
[27] Y. Shen, E. C. Martínez, and C. Rosales-Guzmán, ACS Photonics **9**, 296 (2022).
[28] D. Sugic, R. Droop, E. Otte, D. Ehrmanntraut, F. Nori, J. Ruostekoski, C. Denz, and M. R. Dennis, Nature Communications **12**, 1 (2021).
[29] R. Gutiérrez-Cuevas and E. Pisanty, Journal of Optics **23**, 024004 (2021).
[30] K. M. Song, J.-S. Jeong, B. Pan, X. Zhang, J. Xia, S. Cha, T.-E. Park, K. Kim, S. Finizio, J. Raabe, *et al.*, Nature Electronics **3**, 148 (2020).
[31] S. Li, W. Kang, X. Zhang, T. Nie, Y. Zhou, K. L. Wang, and W. Zhao, Materials Horizons **8**, 854 (2021).
[32] A. J. Nederveen and Y. V. Nazarov, Phys. Rev. Lett. **82**, 406 (1999).
[33] J. Sampaio, V. Cros, S. Rohart, A. Thiaville, and A. Fert, Nature Nanotechnology **8**, 839 (2013).
[34] A. Sonntag, J. Hermenau, S. Krause, and R. Wiesendanger, Phys. Rev. Lett. **113**, 077202 (2014).
[35] C. Reichhardt, D. Ray, and C. J. O. Reichhardt, Phys. Rev. Lett. **114**, 217202 (2015).
[36] J. Hagemeister, N. Romming, K. Von Bergmann, E. Vedmedenko, and R. Wiesendanger, Nature Communications **6**, 1 (2015).
[37] H. Oike, A. Kikkawa, N. Kanazawa, Y. Taguchi, M. Kawasaki, Y. Tokura, and F. Kagawa, Nature Physics **12**, 62 (2016).
[38] A. O. Leonov, Y. Togawa, T. L. Monchesky, A. N. Bogdanov, J. Kishine, Y. Kousaka, M. Miyagawa, T. Koyama, J. Akimitsu, T. Koyama, K. Harada, S. Mori, D. McGrouther, R. Lamb, M. Krajnak, S. McVitie, R. L. Stamps, and K. Inoue, Phys. Rev. Lett. **117**, 087202 (2016).
[39] S. Rohart, J. Miltat, and A. Thiaville, Phys. Rev. B **93**, 214412 (2016).
[40] J. Wild, T. N. Meier, S. Pöllath, M. Kronseder, A. Bauer, A. Chacon, M. Halder, M. Schowalter, A. Rosenauer, J. Zweck, *et al.*, Science Advances **3**, e1701704 (2017).
[41] D. Cortés-Ortuño, W. Wang, M. Beg, R. A. Pepper, M.-A. Bisotti, R. Carey, M. Vousden, T. Kluyver, O. Hovorka, and H. Fangohr, Scientific Reports **7**, 1 (2017).
[42] X. Yu, D. Morikawa, T. Yokouchi, K. Shibata, N. Kanazawa, F. Kagawa, T.-h. Arima, and Y. Tokura, Nature Physics **14**, 832 (2018).
[43] S.-G. Je, H.-S. Han, S. K. Kim, S. A. Montoya, W. Chao, I.-S. Hong, E. E. Fullerton, K.-S. Lee, K.-J. Lee, M.-Y. Im, and J.-I. Hong, ACS Nano **14**, 3251 (2020).
[44] K. Karube, J. S. White, V. Ukleev, C. D. Dewhurst, R. Cubitt, A. Kikkawa, Y. Tokunaga, H. M. Rønnow, Y. Tokura, and Y. Taguchi, Phys. Rev. B **102**, 064408 (2020).
[45] K. Wang, Y. Zhang, V. Bheemarasetty, S. Zhou, S.-C. Ying, and G. Xiao, Nature Communications **13**, 722 (2022).
[46] P. Shi, L. Du, and X. Yuan, Nanophotonics **10**, 3927 (2021).
[47] X. Li, T.-H. Lan, C.-H. Tien, and M. Gu, Nature communications **3**, 998 (2012).
[48] H. Ren, W. Shao, Y. Li, F. Salim, and M. Gu, Science advances **6**, eaaz4261 (2020).
[49] N. Mao, G. Zhang, Y. Tang, Y. Li, Z. Hu, X. Zhang, K. Li, K. Cheah, and G. Li, Proceedings of the National Academy of Sciences **119**, e2204418119 (2022).
[50] Y. Bao, L. Wen, Q. Chen, C.-W. Qiu, and B. Li, Science Advances **7**, eabh0365 (2021).
[51] N. A. Rubin, A. Zaidi, A. H. Dorrah, Z. Shi, and F. Capasso, Science Advances **7**, eabg7488 (2021).
[52] Q. Song, X. Liu, C.-W. Qiu, and P. Genevet, Applied Physics Reviews **9**, 011311 (2022).
[53] B. Göbel, I. Mertig, and O. A. Tretiakov, Physics Reports **895**, 1 (2021).

[54] See Supplemental Material at [url] for generalised vectorial diffraction theory for the generation of arbitrary 3D vectorial fields, details of different types of skyrmions, Amplitude and phase for skyrmion generation, disorder-induce phase transition for the other five classes of optical skyrmionsl, disorder-induced phase transition with different sets of random variables, a comparison of the topological protection for six classes of skyrmions and modelling the random medium, which includes Refs. [48,53,55]

[55] X. Zhang, Y. Zhou, K. M. Song, T.-E. Park, J. Xia, M. Ezawa, X. Liu, W. Zhao, G. Zhao, and S. Woo, Journal of Physics: Condensed Matter **32**, 143001 (2020).

[56] N. Yu, P. Genevet, M. A. Kats, F. Aieta, J.-P. Tetienne, F. Capasso, and Z. Gaburro, Science **334**, 333 (2011).

[57] D. Lin, P. Fan, E. Hasman, and M. L. Brongersma, Science **345**, 298 (2014).

[58] A. Arbabi, Y. Horie, M. Bagheri, and A. Faraon, Nature Nanotechnology **10**, 937 (2015).

[59] J. B. Mueller, N. A. Rubin, R. C. Devlin, B. Groever, and F. Capasso, Physical Review Letters **118**, 113901 (2017).

[60] R. C. Devlin, A. Ambrosio, N. A. Rubin, J. B. Mueller, and F. Capasso, Science **358**, 896 (2017).

[61] H. Ren, X. Fang, J. Jang, J. Bürger, J. Rho, and S. A. Maier, Nature Nanotechnology **15**, 948 (2020).

[62] M. Liu, W. Zhu, P. Huo, L. Feng, M. Song, C. Zhang, L. Chen, H. J. Lezec, Y. Lu, A. Agrawal, and T. Xu, Light: Science & Applications **10**, 107 (2021).